CD81 regulates cell migration through its association with Rac GTPase

Emilio Tejera[a,b], Vera Rocha-Perugini[b], Soraya López-Martín[a], Daniel Pérez-Hernández[b,c], Alexia I. Bachir[d], Alan Rick Horwitz[d], Jesús Vázquez[b,c], Francisco Sánchez-Madrid[b,e], and María Yáñez-Mo[a]

[a]Unidad de Investigación, Hospital Santa Cristina and [e]Servicio de Inmunología, Hospital de la Princesa, Instituto de Investigación Sanitaria La Princesa, 2006 Madrid, Spain; [b]Departamento de Biología Vascular e Inflamación, Centro Nacional de Investigaciones Cardiovasculares, 28029 Madrid, Spain; [c]Cardiovascular Proteomics Laboratory, Centro de Biología Molecular "Severo Ochoa"–Consejo Superior de Investigaciones Científicas, 28049 Cantoblanco, Madrid, Spain; [d]Department of Cell Biology, University of Virginia School of Medicine, Charlottesville, VA 22908

ABSTRACT **CD81 is a member of the tetraspanin family that has been described to have a key role in cell migration of tumor and immune cells. To unravel the mechanisms of CD81-regulated cell migration, we performed proteomic analyses that revealed an interaction of the tetraspanin C-terminal domain with the small GTPase Rac. Direct interaction was confirmed biochemically. Moreover, microscopy cross-correlation analysis demonstrated the in situ integration of both molecules into the same molecular complex. Pull-down experiments revealed that CD81-Rac interaction was direct and independent of Rac activation status. Knockdown of CD81 resulted in enhanced protrusion rate, altered focal adhesion formation, and decreased cell migration, correlating with increased active Rac. Reexpression of wild-type CD81, but not its truncated form lacking the C-terminal cytoplasmic domain, rescued these effects. The phenotype of CD81 knockdown cells was mimicked by treatment with a soluble peptide with the C-terminal sequence of the tetraspanin. Our data show that the interaction of Rac with the C-terminal cytoplasmic domain of CD81 is a novel regulatory mechanism of the GTPase activity turnover. Furthermore, they provide a novel mechanism for tetraspanin-dependent regulation of cell motility and open new avenues for tetraspanin-targeted reagents by the use of cell-permeable peptides.**

Monitoring Editor
Denise Montell
Johns Hopkins University

Received: Sep 4, 2012
Revised: Nov 16, 2012
Accepted: Dec 5, 2012

INTRODUCTION

Tetraspanins are involved in adhesion and migration processes, such as leukocyte extravasation and cancer invasion (Yáñez-Mó *et al.*, 2001a, 2001b, 2009; Hemler, 2003; Tarrant *et al.*, 2003; Barreiro *et al.*, 2005; Charrin *et al.*, 2009), and are promising targets for cancer therapeutics (Sala-Valdes *et al.*, 2012).

Multiple studies have provided evidence that tetraspanins regulate cell migration. Initial reports used antitetraspanin antibodies (Lagaudriere-Gesbert *et al.*, 1997; Yáñez-Mó *et al.*, 1998): anti-CD81 antibodies inhibited α6β1-induced migration (Domanico *et al.*, 1997), and anti-CD151 and anti-CD81 antibodies reduced migration of endothelial or epithelial cells (Yáñez-Mó *et al.*, 1998; Penas *et al.*, 2000). More recently, anti-CD81 antibodies were found to ameliorate autoimmune encephalomyelitis by blocking monocyte transmigration (Dijkstra *et al.*, 2008).

Genetic studies also support this role for tetraspanins. Small interfering RNA (siRNA)-mediated deletion of CD9 and CD151 enhanced primary melanocyte motility (Garcia-Lopez *et al.*, 2005), whereas targeting of CD151 enhanced melanoma cell migration (Hong *et al.*, 2006). CD82 overexpression suppressed the migration of oligodendrocyte precursors (Mela and Goldman, 2009). In the immune system, CD81 regulates the migration and trafficking of

This article was published online ahead of print in MBoC in Press (http://www.molbiolcell.org/cgi/doi/10.1091/mbc.E12-09-0642) on December 21, 2012.

Address correspondence to: María Yáñez-Mó (myanez.hlpr@salud.madrid.org).

Abbreviations used: ANOVA, analysis of variance; EGF, epidermal growth factor; FBS, fetal bovine serum; FDR, false discovery rate; FRET, fluorescence resonance energy transfer; GFP, green fluorescent protein; GST, glutathione *S*-transferase; HUVEC, human umbilical vein endothelial cells; LC-MS/MS, liquid chromatography–tandem mass spectrometry; NA, numerical aperture; PBS, phosphate-buffered saline; PKC, protein kinase C; siRNA, small interfering RNA; TAMRA, tetramethylrhodamine; TEM, tetraspanin-enriched microdomains; TIRFM, total internal reflection microscopy; UTR, untranslated region.

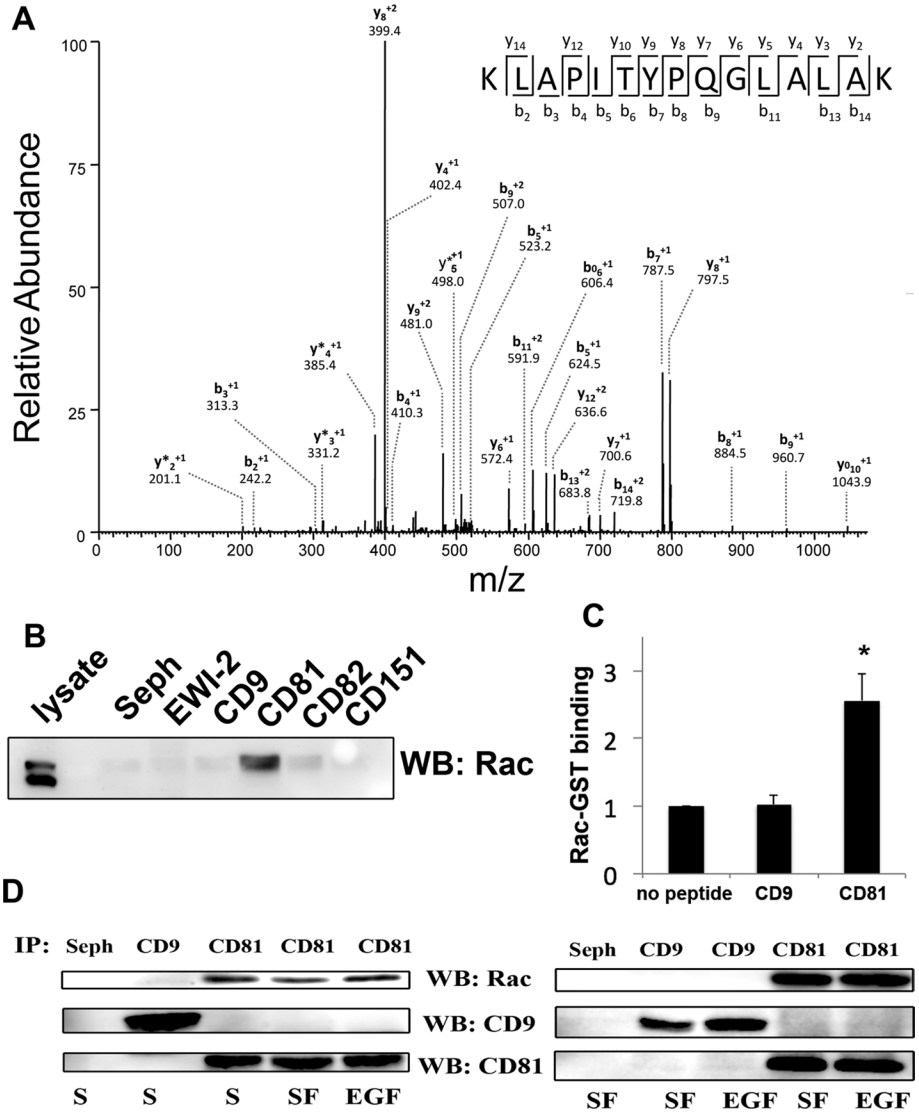

FIGURE 1: The C-terminal domain of CD81 associates with the GTPase Rac1. (A) Primary T-lymphoblast lysates were incubated with biotinylated peptides of the C-terminal cytoplasmic domain of CD81. Pull downs were digested, and the resulting peptides were identified by high-throughput MS. (A) Representative MS/MS spectrum of a Rac2 peptide. (B) Rac immunoblot of HEK lysates pulled down with biotinylated peptides corresponding to C-terminal domains of tetraspanins CD9, CD81, CD82, and CD151, and tetraspanin-associated receptor EWI-2. Sepharose-negative control and total cell lysates are also shown. (C) Rac1-GST protein produced in *E. coli* was incubated with CD9 or CD81 C-terminal biotinylated peptides. GST binding was quantified by chemiluminescence. Data correspond to five independent experiments (mean ± SEM) *, $p < 0.05$ in one-way ANOVA. (D) Lysates from SUM159 (left) and HUVEC (right), either serum-starved (SF) and exposed to EGF (100 ng/ml) for 5 min (EGF) or maintained in standard serum culture conditions (S) were immunoprecipitated with anti-CD81 (5A6) or and anti-CD9 (VJ1/20). Membranes were immunoblotted for Rac, CD81, and anti-CD9.

natural killer (Kramer *et al.*, 2009) and dendritic (Nattermann *et al.*, 2006) cells, while CD9/CD81 double-knockout mice show defects in macrophage cell motility (Takeda *et al.*, 2008).

Tetraspanins are highly hydrophobic proteins that cross the cellular membrane four times, displaying N-terminal and C-terminal cytoplasmic domains. Tetraspanins structure tetraspanin-enriched microdomains (TEMs) at the plasma membrane that organize transmembrane proteins, including integrins, immunoglobulin-like adhesion molecules and metalloproteinases, and signaling effectors (Yáñez-Mó *et al.*, 2009, 2011). Integrin insertion in TEMs enhances integrin's avidity for ligands and regulates outside-in signaling (Berditchevski and Odintsova, 1999), including the activation of FAK, Src, p130^{cas} and paxillin (Yamada *et al.*, 2008), protein kinase B, endothelial nitric-oxide synthase, and the small GTPases Rac1 and Cdc42 (Takeda *et al.*, 2007).

Emerging evidence suggests that tetraspanins also interact with different cytoplasmic molecules, facilitating the activation of signaling cascades. At least five tetraspanins—CD9, CD63, CD81, CD151, and A15/TALLA/Tspan7—associate with type II phosphatidylinositol 4-kinase (Berditchevski *et al.*, 1997; Yauch and Hemler, 2000). Tetraspanin association to PI4K may play a role in cell migration (Mazzocca *et al.*, 2008), bacterial infection (Tham *et al.*, 2010), and tumor cell proliferation (Carloni *et al.*, 2004). When activated, protein kinase C (PKC) associates with CD9, CD53, CD81, CD82, and CD151 (Zhang *et al.*, 2001a), and PKC-mediated phosphorylation was shown to be necessary for α3-integrin–dependent signaling to FAK, p130^{cas}, and paxillin during spreading and migration (Zhang *et al.*, 2001b). The C-terminal cytoplasmic domain of CD63 binds to the adaptor protein syntenin-1 (Latysheva *et al.*, 2006) and that of CD81 to 14-3-3 proteins (Clark *et al.*, 2004). Tetraspanins connect to the actin cytoskeleton through ezrin, radixin, and moesin (ERM) proteins (Sala-Valdes *et al.*, 2006), and tetraspanin-mediated signaling may control actin polymerization and remodeling. However, the precise mechanisms through which tetraspanins control cell migration remain largely unexplored.

In this study, we performed pull-down assays using the cytoplasmic C-terminus tail of CD81 as bait, followed by high-throughput protein identification by mass spectrometry, to identify new intracellular interacting partners of tetraspanins implicated in the regulation of actin dynamics and cell migration. We found that tetraspanin CD81 associates with the small GTPase Rac. We also demonstrate that CD81 interaction with Rac limits the GTPase activation within the plasma membrane, providing an unexpected novel regulatory mechanism of Rac activity turnover.

RESULTS

CD81 associates with Rac1 through its cytoplasmic C-terminal region

Searching for novel interactions of CD81 implicated in cell migration, we performed mass spectrometry using pull downs of T-lymphoblast cell lysates with biotinylated peptides corresponding to the C-terminal cytoplasmic region of CD81 as bait. The analysis identified two peptides belonging to the GTPase Rac1 and five corresponding to Rac2 (Figure 1A) in the bound fraction. The association of CD81 with Rac was also detected by pull-down assays with

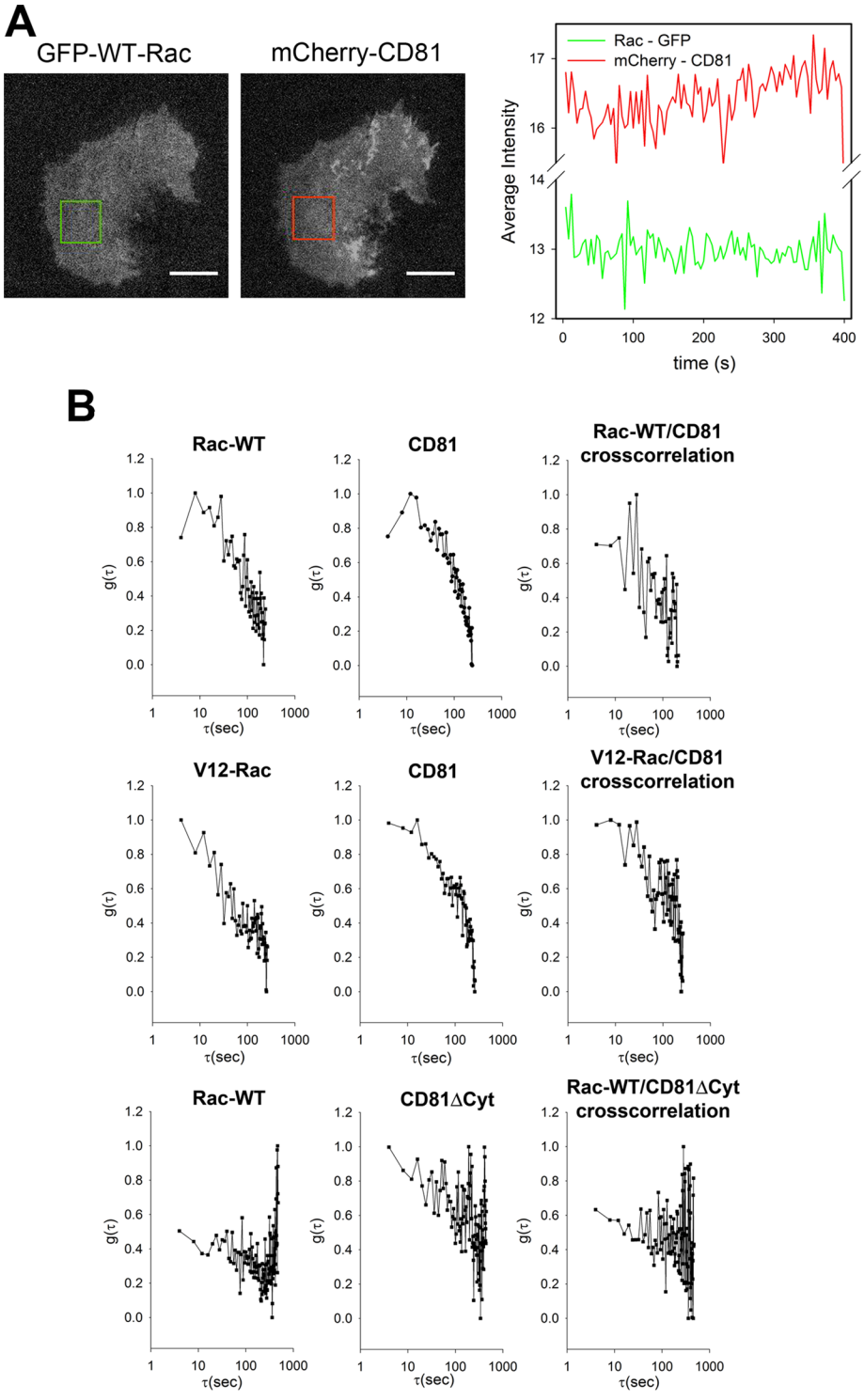

FIGURE 2: CD81 and Rac are found in common molecular complexes. (A) Cross-correlation analysis of TIRFM time-lapse imaging of mCherry-CD81 and GFP-Rac in U2OS cells plated on 2 µg/ml fibronectin. Time series consisted of 100 frames captured at 4-s intervals. A square region (~ 80 µm^2) in the image time series was selected for analysis (highlighted in the example shown). The average intensity of the analyzed regions for both channels showed minimal photobleaching or mechanical drift effects. Scale bars: 10 µm. (B) The auto- and cross-correlation functions are presented on a semilogarithmic scale.

adherent cells (Figure 1B). Interestingly, the C-terminal cytoplasmic regions of the tetraspanins CD9, CD151, and CD82 did not associate with Rac (Figure 1B; unpublished data). Similarly, biotinylated peptides corresponding to the cytoplasmic sequence of other tetraspanin-associated membrane molecules (EWI-2, ICAM-1, VCAM-1) and other membrane receptors (CD147, CD69, CXCR4, CCR7) were unable to pull down Rac (Figure 1B; unpublished data). Direct interaction with the C-terminal sequence of CD81 was confirmed by direct binding of Rac1–glutathione *S*-transferase (GST) protein obtained in *Escherichia coli* cultures (Figure 1C). Interaction between the endogenous molecules was confirmed by coimmunoprecipitation in serum-starved, serum-induced, or epidermal growth factor (EGF)-stimulated primary human umbilical vein endothelial cells (HUVEC) or SUM159 breast carcinoma cells (Figure 1D).

CD81-Rac molecular complexes were detected in situ by total internal reflection microscopy (TIRFM)-based fluorescence image cross-correlation analysis of mCherry-CD81 and green fluorescent protein (GFP)-tagged wild-type Rac (WT-Rac1; Figure 2A). Correlation studies rely on the analysis of fluorescence intensity fluctuations from fluorescently tagged molecules in an image time series. The fluctuations, in this case, likely arise from diffusion and/or membrane binding–unbinding kinetics. The decay of the autocorrelation function for CD81 and wild type Rac (WT-Rac1) indicates that both molecules are producing fluorescence fluctuations over the timescale of the measurement (Figure 2B, top panels). This observation is typical for transmembrane receptors such as CD81, which diffuse in the cell membrane on the seconds timescale (faster than cytosolic proteins), or proteins with slow exchange with the membrane, and suggests that we are measuring a Rac population that is either diffusing in the membrane or exchanging with a membrane-bound complex (Moissoglu *et al.*, 2006).

As we have previously demonstrated, correlation analysis can also be applied to detect molecular complexes (Choi *et al.*, 2011). If two molecules tagged with different fluorophores (e.g., GFP and mCherry) reside within the same molecular complex, they will produce similar temporal fluorescence intensity fluctuation patterns, which will be revealed by calculating the cross-correlation function (see *Materials and Methods*; Wiseman *et al.*, 2004; Brown *et al.*, 2006; Digman *et al.*, 2009). In the absence of a complex, the intensity fluctuations are independent, and the cross-correlation function will be featureless and indistinguishable from the noise level. The cross-correlation function of CD81 and WT-Rac-1 therefore confirms that the membrane-targeted Rac1 resides with CD81 in the same complex. CD81 also showed high cross-correlation with V12-Rac, a

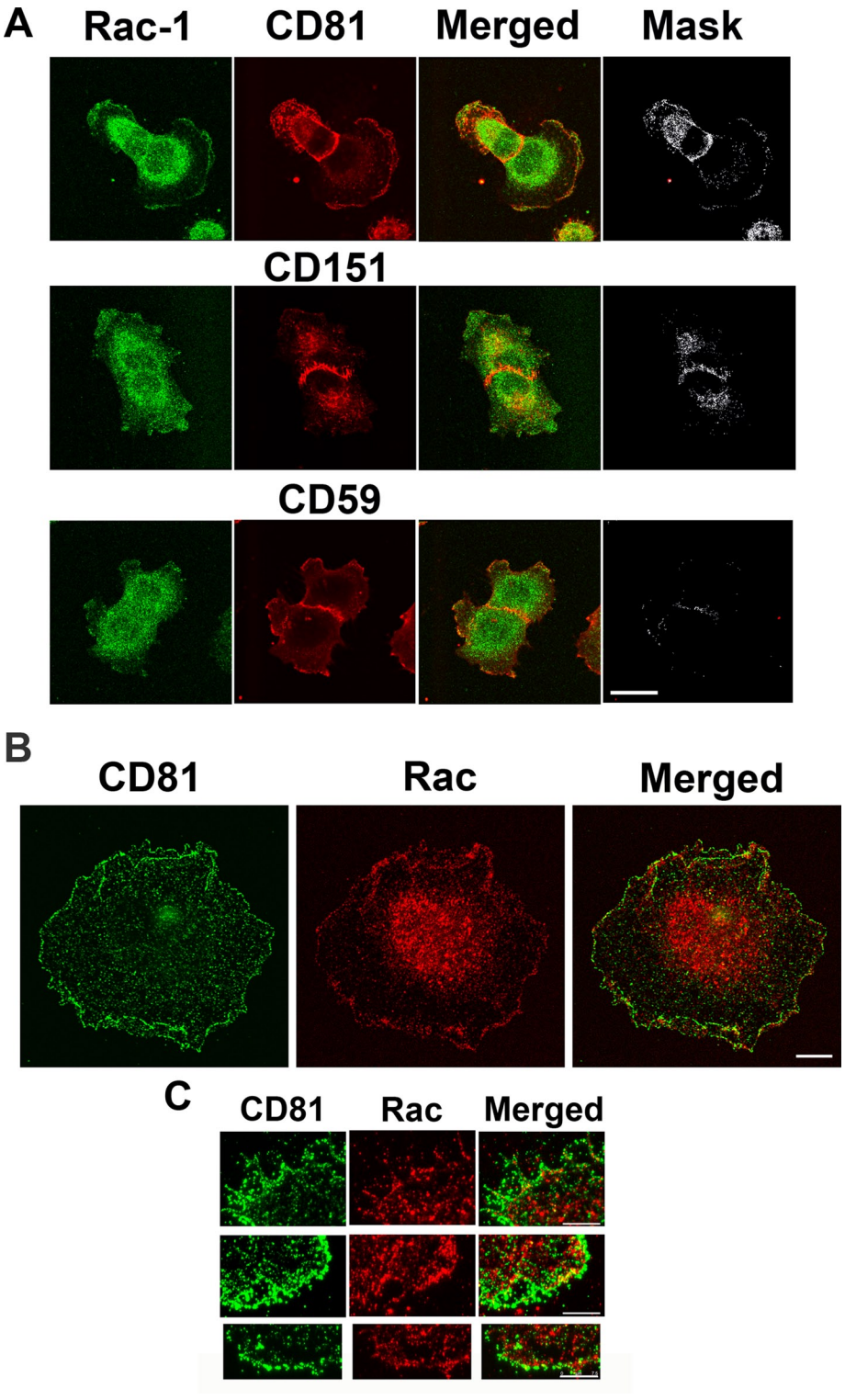

FIGURE 3: Endogenous CD81 colocalizes with Rac. (A) SUM159 cells were fixed after 5 min of EGF stimulation (100 ng/ml), permeabilized, and costained for Rac1 and CD81, CD151, or CD59. A confocal plane of both channels is shown together with the merged image and an image overlaid with the colocalization mask in white. Scale bar: 20 μm. (B and C) HUVEC cells were plated onto 10 μg/ml of fibronectin for 30 min, fixed, permeabilized, and stained for Rac and CD81. Samples were analyzed by (B) confocal microscopy (maximal projection) or (C) TIRFM. Scale bar: (B) 10 μm; (C) 7.5 μm.

constitutively active mutant of Rac (Figure 2B, middle panels). Coexpression of WT-Rac with a CD81 mutant lacking the cytoplasmic region (CD81-ΔCyt) resulted in reduced Rac autocorrelation, suggesting a faster exchange of the GTPase with the membrane. Moreover, both molecules showed no detectable cross-correlation, further indicating that Rac specifically binds to the CD81 C-terminal region (Figure 2B, bottom panels).

CD81 colocalizes with Rac1 and localizes anterior to nascent adhesions at the leading edge of migrating cells

We next studied the subcellular localization of CD81/Rac complexes in live cells. Stimulation of SUM159 cells or HUVEC with EGF induced partial colocalization of endogenous Rac and CD81 at the cell edge (Figure 3, A and B), and similar results were observed during cell spreading (unpublished data). Colocalization at the leading lamella was not observed for tetraspanin CD151, which concentrated at cell–cell contacts, or for the glycophosphatidylinositol (GPI)-linked receptor CD59 (Figure 3A). Analysis of similar samples using TIRFM, illuminating only ~100 nm of the ventral surface of the cell, revealed the colocalization of CD81 and Rac1 at the edges of HUVEC cells (Figure 3C).

Loading of Rac with GTP is normally concomitant with its translocation to the plasma membrane. To determine whether association of CD81 with Rac depends on the activation state of the GTPase, we loaded SUM159 cell lysates with an excess of GDP or the nonhydrolyzable GTP analogue GTP-γS. CD81-biotinylated peptides pulled down similar amounts of Rac regardless of the GTP or GDP load, suggesting that CD81 association with Rac is independent of the Rac activation state (Figure 4A).

The dynamic behavior of the CD81/Rac complexes in migrating cells was analyzed with a Förster resonance energy transfer (FRET)-based Raichu-Rac plasmid that allows the dynamic visualization of Rac activity (Ouyang *et al.*, 2008). In human microvascular endothelial cells cotransfected with DsRed-CD81 and Raichu-Rac, EGF stimulation induced a clear colocalization of Rac activity with CD81 at the leading edges of the cells (Figure 4B and Supplemental Video S1). In resting cells, FRET signal was almost undetectable. To define more precisely the location of CD81-Rac complexes at the leading lamella, we cotransfected cells with AqGFP-CD81 and orange-paxillin and monitored them using time-lapse TIRFM. CD81 concentrated at the edges of the cells (Figure 4C, arrowhead, and Video S2), ahead of the nascent adhesions marked by paxillin (Figure 4C, arrow) suggesting that CD81 may prime these foremost areas for Rac activation.

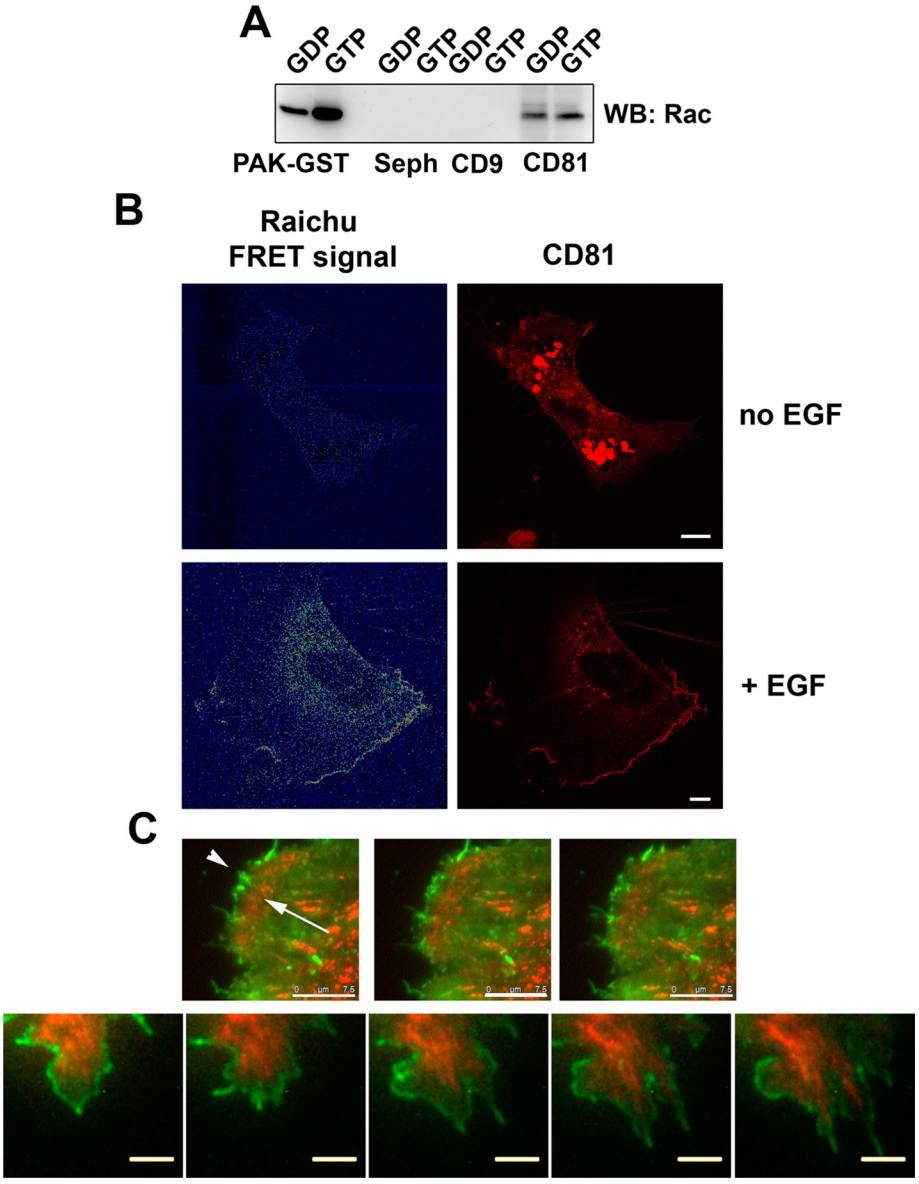

FIGURE 4: CD81 colocalizes with Rac activity anterior to nascent adhesions at the leading edge of migrating cells. (A) SUM159 cell lysates were loaded with 50 nM of GTP-γS or GDP before pull down with CD81 and CD9 C-terminal domain biotinylated peptides. GTP-γS/GDP Rac loading was assessed by pull down with GST-PAK-CRIB. (B) HMEC-1 cells were cotransfected with DsRed-CD81 and ECFP/Ypet Raichu-Rac. FRET signal for Raichu-Rac (left) and CD81 (right) are shown for untreated cells or cells stimulated with EGF (100 ng/ml). Scale bars: 10 μm. (C) HMEC-1 cells were cotransfected with Aq-GFP-CD81 and mOrange-paxillin and observed using TIRFM. Representative time points are shown. Arrowhead points to CD81 signal at the leading edge, while the arrow highlights the position of the nascent adhesions containing paxillin. Scale bars: 7.5 μm (top), 5 μm (bottom).

CD81 controls Rac activation dynamics during cell adhesion and migration

The functional significance of the CD81/Rac interaction was explored in cells with reduced endogenous CD81 expression by transfection of two different siRNA sequences: one against the coding sequence and one against the 3′ untranslated region (3′UTR; see *Material and Methods*). After 48 h of siRNA transfection, down-regulation was assessed by flow cytometry and Western blotting (Figure 5, A and B); experiments were performed only when down-regulation was higher than 50%. We monitored the subcellular location of GFP-coupled Rac1 during migration on fibronectin in control cells and CD81-depleted cells (Figure 5C). Rac concentrated at the leading edge in both conditions, suggesting that CD81 is not required for Rac translocation to the plasma membrane (Figure 5C and Video S3).

Interestingly, active (GTP-bound) Rac levels, as detected by pull down with GST-PAK-CRIB, were significantly higher in unstimulated CD81-silenced cells ($p < 0.05$ in Student's *t* test). Moreover, in CD81-silenced cells, Rac-GTP levels remained largely unaffected by EGF stimulation. Indeed, Rac activity remained high and almost constant, being also significantly higher at 30 min of EGF stimulation compared with control cells ($p < 0.05$ in Student's *t* test). In contrast, no significant differences were observed in RhoA activity (detected with GST-C21), which was only slightly reduced in CD81-silenced cells (Figure 5D).

Cell protrusion during spreading depends mainly on Rac-induced actin polymerization (Choi *et al.*, 2008). Consistent with the higher levels of activated Rac, CD81-deficient cells displayed a faster rate of protrusion and spreading than control cells (Figure 6, A and B). Importantly, this effect was rescued using full-length CD81 but not with the C-terminus truncated form (CD81-ΔCyt) fused to GFP. Moreover, overexpression of WT-CD81 had the opposite effect, slowing cell protrusion (Figure 6A).

The effects of CD81 depletion in actin polymerization and adhesion formation were visualized by staining F-actin and the adhesion protein paxillin in control and CD81-deficient cells. To normalize cell morphology, we used micropatterned substrates (Thery *et al.*, 2006) that permit averaging the staining of multiple cells with the same morphology, as well as analyzing the response to geometric cues (Tan *et al.*, 2004; Figure 6C). CD81-depleted cells showed increased paxillin staining of focal adhesions (Figure 6C). Interestingly, adhesions in control cells were restricted to the rim of the lamellar edge, but formed in a broader region in CD81-silenced cells. CD81 depletion also induced a defective cell polarization in both F-actin and focal adhesions in polarizing micropatterns. CD81 silencing in primary HUVECs plated onto fibronectin also increased the size of focal adhesions (Figure 6D), an effect reverted by cotransfection with full-length CD81, but not with CD81-ΔCyt-GFP. It has been reported that protrusion rate presents a direct correlation with adhesion assembly rate (Choi *et al.*, 2008). We analyzed adhesion assembly and disassembly rates in cells interfered for CD81, with or without reconstitution of the expression with a complete or truncated CD81 form. For adhesion assembly rate, results were consistent with protrusion rates: silencing of CD81 accelerated adhesion assembly compared with control cells, and this phenotype was rescued by complete CD81 but not by the truncated form (Figure 6E). In contrast, no

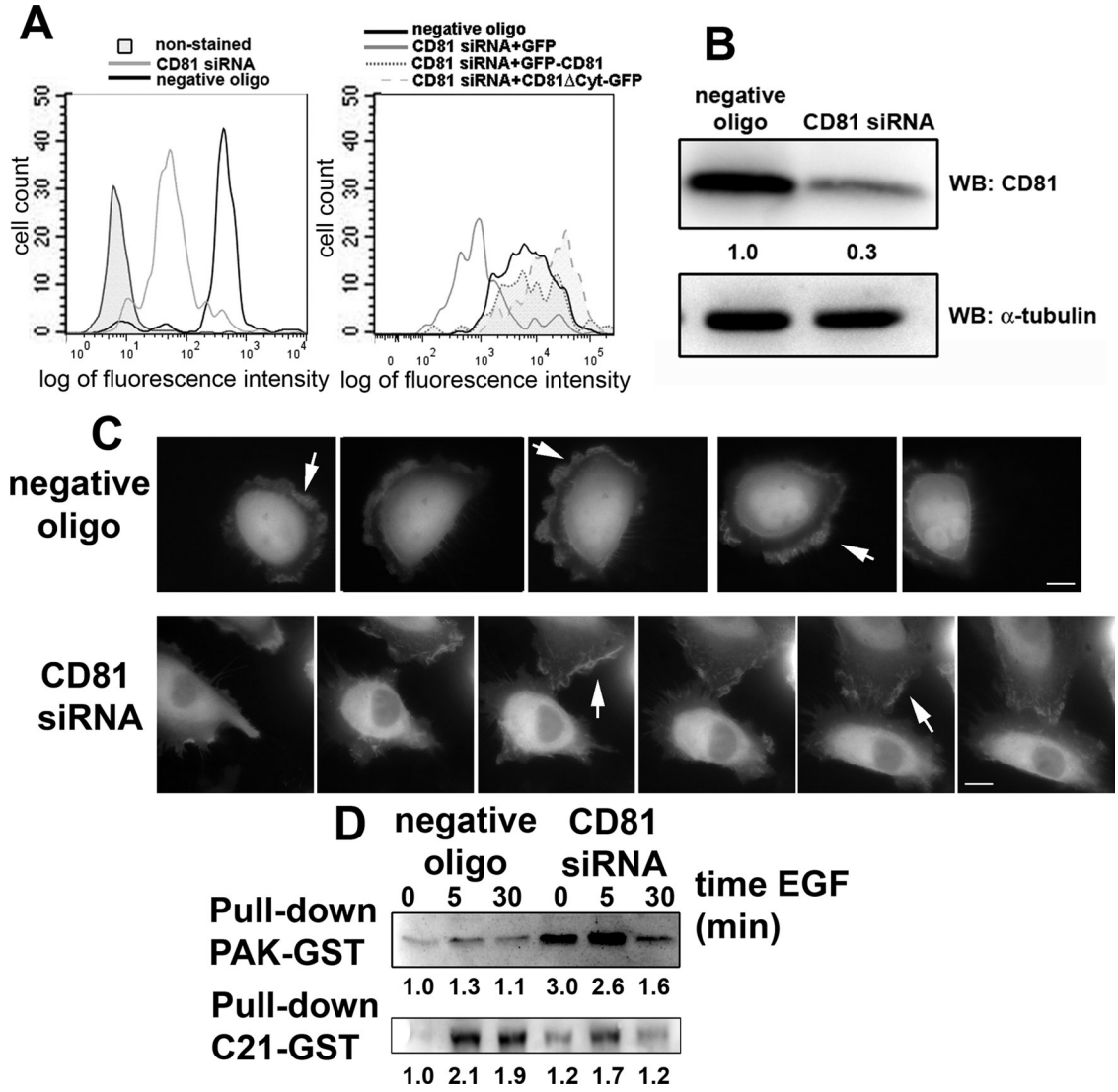

FIGURE 5: CD81 silencing does not impair Rac translocation to cell membrane but increases Rac activation. (A) Flow cytometry analyses of CD81 silencing. SUM159 cells were transfected with negative oligo or CD81 siRNA (b sequence) and stained for CD81 (left). Negative control, cells stained with the secondary antibody only (filled histogram) are shown for reference. For rescue experiments (right), cells were cotransfected with negative oligonucleotide (thick black line) or CD81c sequence siRNA and plasmid DNA encoding GFP (thin gray line), GFP-CD81 (gray dotted line), or truncated mutant CD81-ΔCyt-GFP (gray dashed line). (B) Western blot analyses of CD81 silencing. SUM159 cells were transfected with negative oligo or CD81 siRNA, and total cell lysates were blotted for CD81 content. α-Tubulin is shown as loading control. (C) SUM159 cells were cotransfected with negative oligonucleotide or CD81siRNA together with GFP-wild-type-Rac1. Time-lapse images were acquired using wide-field fluorescence video microscopy. Maximal projections of representative time points are shown. Arrows point to Rac accumulation at the lamella of the migrating cells. Scale bars: 10 μm. (D) SUM159 cells were transfected with negative oligonucleotide or CD81 siRNA, serum-starved, and stimulated with EGF (100 ng/ml) at the indicated times. Rac and Rho activation were analyzed by pull-down assays with GST-PAK-CRIB or GST-C21, respectively. Blots are representative from at least three independent experiments.

statistically significant differences were found between any of the groups for the rate of adhesion disassembly, indicating CD81 is able to modify the turnover of focal adhesions, exerting an effect on the assembly of the adhesions, but not on the disassembly.

To directly corroborate that CD81 regulated Rac activation by their interaction through the C-terminal cytosolic domain of the tetraspanin, we incubated cells with a fluorescently labeled, cell-permeable peptide corresponding to the C-terminal sequence of CD81 or with a scrambled combination of the same eight amino acids as a control. These peptides were readily internalized; at 1 h after incubation, 100% of the cells were fluorescently labeled. The mean fluorescence intensity of the cells increased up to 3 h and declined thereafter, although 100% of the cells retained detectable fluorescence after 24 h (Figure 7A; unpublished data). Both peptides faintly labeled the plasma membrane and strongly accumulated at intracellular vesicles (Figure 7B). Incubation with the CD81 C-terminal peptide, but not with the control, increased the basal levels of Rac activity, but prevented its activation in response to EGF (Figure 7C), similar to what was observed when silencing CD81 in these cells. In the same manner, CD81 C-terminal peptides induced a higher protrusion rate

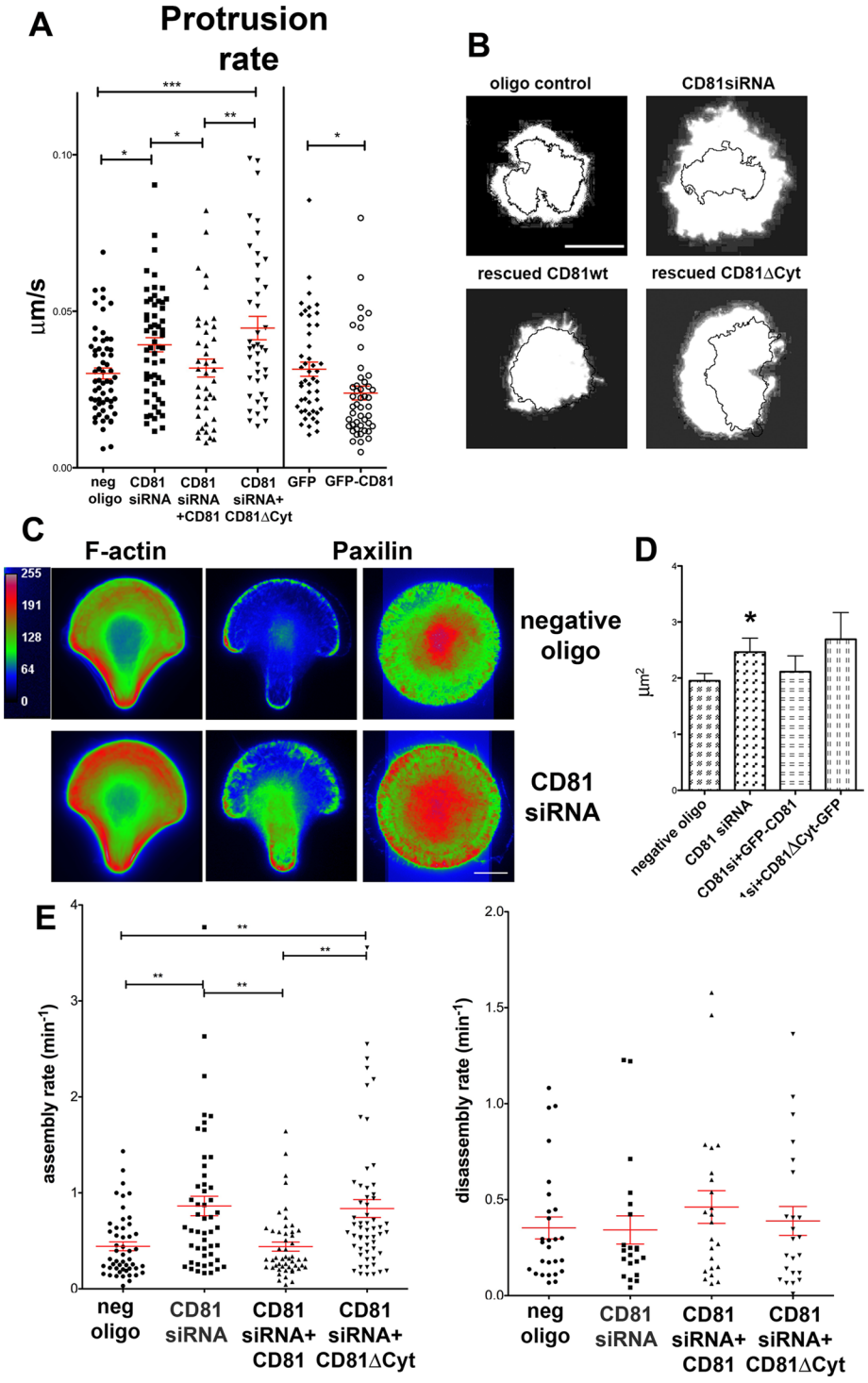

FIGURE 6: CD81 down-regulation increases protrusion rate and focal adhesion formation. (A) SUM159 cells were transfected with negative oligonucleotide or CD81 siRNA, together with GFP, GFP-CD81, or the GFP-tagged truncated C-terminal deletion form of CD81. In parallel experiments, cells were transfected with GFP or GFP-CD81. Protrusion rate (µm/s) was analyzed in TIRF time-lapse sequences of cells spreading on 10 µg/ml fibronectin. Data represent kymographs from three independent experiments (mean ± SEM). *, $p < 0.05$; **, $p < 0.01$; and ***, $p < 0.001$ in one-way ANOVA (silencing and rescue experiments); *, $p < 0.05$ in Student's t test for overexpression experiments. (B) Examples of cell spreading measured in (A). Binary images show the total area of spreading at 5 min, while the linear outline corresponds to the cell perimeter at time 0. Scale bar: 10 µm. (C) SUM159 cells were transfected with negative oligonucleotide or CD81 siRNA and seeded onto micropatterned slides. After 3 h of adhesion, samples were fixed, permeabilized, and stained for paxillin or F-actin. Images displayed are the average projections, in pseudocolor intensity scale, of more than 20 cells acquired in a wide-field fluorescence microscope. Scale bar: 10 µm. (D) Primary HUVECs were transfected with negative oligonucleotide or CD81 siRNA, together with GFP, GFP-CD81, or the GFP-tagged truncated C-terminal deletion form of CD81, and seeded on 2 µg/ml of fibronectin. Cells were stained for paxillin, and the area of focal adhesions (µm²) was quantified. Data are means ± SEM of measurements from three independent experiments. *, $p < 0.05$ in one-way ANOVA. (E) Cells were transfected with mOrange-paxillin together with negative oligonucleotide or CD81 siRNA and GFP, GFP-CD81, or the GFP-tagged truncated C-terminal deletion form of CD81, then allowed to spread on 10 µg/ml fibronectin, and adhesion assembly and disassembly (depicted by paxillin) were analyzed in TIRFM time-lapse sequences. Data are means ± SEM of measurements from three independent experiments. **, $p < 0.01$ in one-way ANOVA.

(Figure 7D) and increased the cell area after spreading (Figure 7E).

Therefore our data suggest that perturbation of the Rac-CD81 interaction alters the normal Rac activation/inactivation cycle, resulting in increased but delocalized protrusion and increased adhesion formation. Time-lapse video microscopy experiments revealed that these alterations in Rac activity by CD81 depletion decreased the rate of cell migration, an effect avoided by cotransfection with full-length CD81 but not with the CD81ΔCyt mutant (Figure 8, A and B). Again, overexpression of WT-CD81 had the opposite effect, facilitating cell migration (Figure 8C), while treatment of cells with the permeable peptides recapitulated the phenotype of CD81 siRNA depletion, slowing cell motility (Figure 8D).

In sum, the binding of Rac to the C-terminal cytoplasmic domain of CD81 is an important mechanism responsible for tetraspanin regulation of cell migration. Furthermore, insertion into TEM emerges as a novel regulatory mechanism for Rac activity turnover.

DISCUSSION

Tetraspanins have been implicated in the regulation of cell migration in different biological scenarios. The current view favors an interpretation of these results based on the interaction of tetraspanins with other membrane molecules in tetraspanin-enriched microdomains (Berditchevski, 2001; Yáñez-Mó *et al.*, 2009). Our study provides the first evidence that CD81 and Rac associate in the same multimolecular complex and emphasizes the role of tetraspanins as direct regulators of signals that control cell migration.

Our results show that CD81 directly binds to Rac proteins. Mass spectrometry

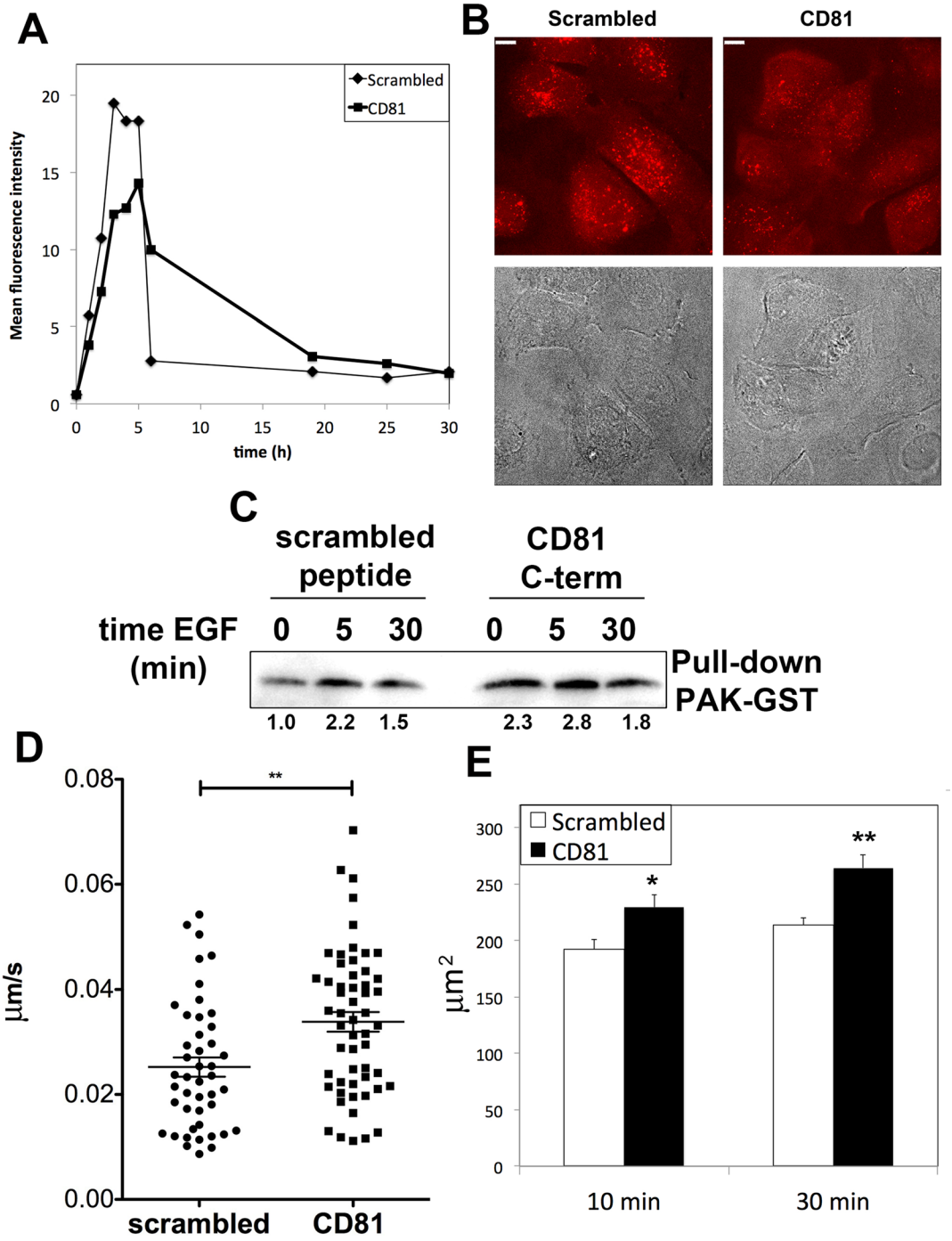

FIGURE 7: A cell-permeable peptide with CD81 C-terminal sequence affects Rac activity. (A) SUM159 cells were incubated with 1 µM of a fluorescently labeled cell-permeable peptide with the sequence of the C-terminal cytoplasmic domain of CD81 or a scrambled version for the indicated times. Cells were trypsinized and incorporation of the peptide analyzed by flow cytometry. (B) SUM159 cells were incubated for 2 h with 1 µM of the permeable peptides containing the sequence of the C-terminal cytoplasmic domain of CD81 or the scrambled version, fixed, and visualized by confocal microscopy. A maximal projection of the confocal stacks together with a phase-contrast image is shown. Scale bars: 7.5 µm. (C) SUM159 cells were serum-starved, incubated for 2 h with 1 µM of the permeable peptides containing the sequence of the C-terminal cytoplasmic domain of CD81 or the scrambled version, and stimulated with EGF (100 ng/ml) at the indicated times. Rac activation was analyzed by pull-down assays with GST-PAK-CRIB. (D) SUM159 cells were incubated for 2 h with 1 µM of the permeable peptides containing the sequence of the C-terminal cytoplasmic domain of CD81 or the scrambled version. Protrusion rate (µm/s) was analyzed in TIRFM time-lapse sequences in cells spreading on 10 µg/ml fibronectin. Data represent kymographs from three independent experiments (mean ± SEM). **, $p < 0.01$ in Student's *t* test. (E) SUM159 cells were incubated for 2 h with 1 µM of the permeable peptides containing the sequence of the C-terminal cytoplasmic domain of CD81 or the scrambled version, trypsinized, and plated onto 10 µg/ml fibronectin; fixed at indicated times; and stained for F-actin. Data represent the cell average area ± SEM from three independent experiments. *, $p < 0.05$, **, $p < 0.01$ in Student's *t* test.

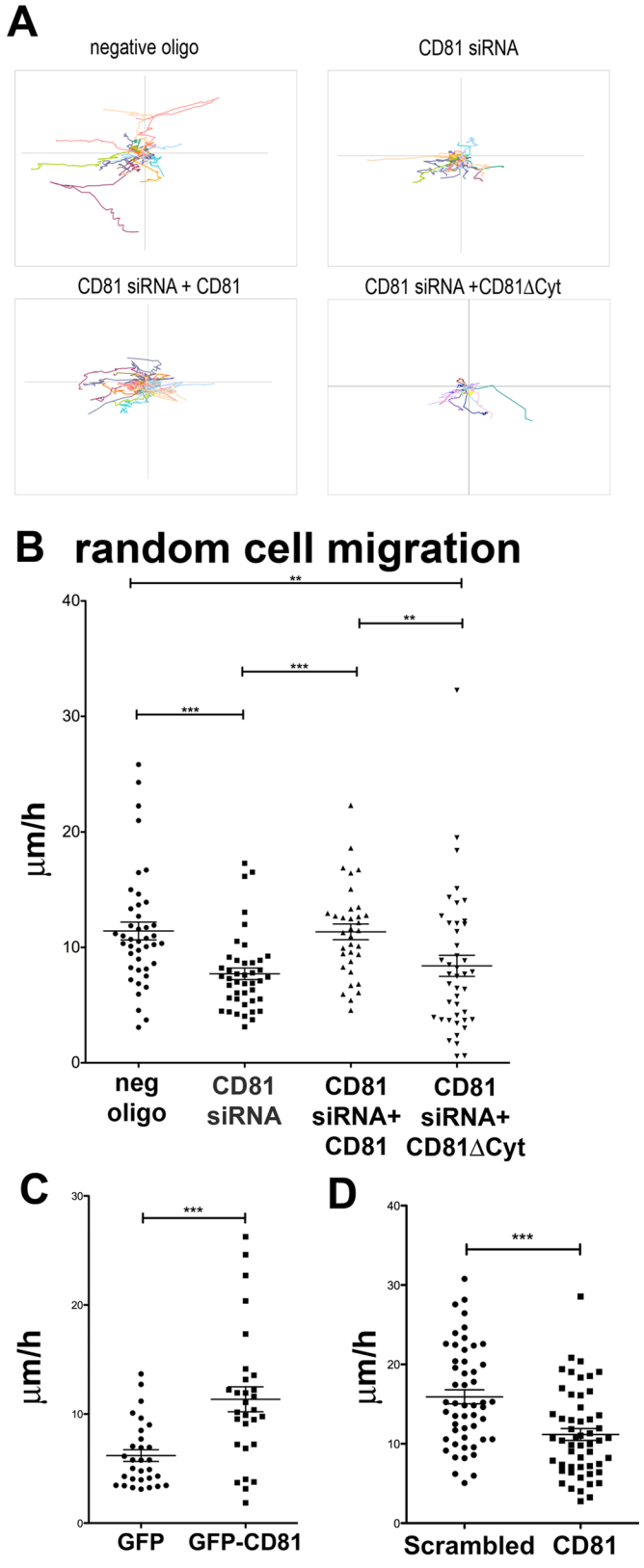

FIGURE 8: CD81 expression levels regulate cell migration
(A) SUM159 cells were transfected with negative oligonucleotide or CD81 siRNA, together with GFP, GFP-CD81, or the GFP-tagged truncated C-terminal deletion form of CD81, and allowed to migrate onto 2 μg/ml fibronectin for 24 h. Charts depict individual tracks in a representative experiment. (B) Individual cell migration speeds are expressed in μm/h. Mean ± SEM from three independent experiments. **, $p < 0.01$; ***, $p < 0.001$ in one-way ANOVA. (C) SUM159 cells were transfected with GFP or GFP-CD81 and allowed to migrate onto 2 μg/ml fibronectin for 24 h. Individual cell migration speeds are expressed in μm/h. Mean ± SEM from three independent experiments. ***, $p < 0.001$ in Student's *t* test. (D) SUM159 cells were preincubated for 1 h with 1 μM of the permeable peptides containing the sequence of the C-terminal cytoplasmic domain of CD81 or the scrambled version and allowed to migrate onto 2 μg/ml fibronectin for 24 h. Individual cell migration speeds are expressed in μm/h. Mean ± SEM from three independent experiments. **, $p < 0.01$ in Student's *t* test.

analyses of CD81 pull downs show a preference for Rac2, which is enriched in T-lymphoblasts, over Rac1 (Guo *et al.*, 2008). These results were corroborated in adherent cells with Rac-1 and by in vitro direct binding of Rac-1 protein produced in bacterial lysates to the C-terminal sequence of CD81. Previous data showed that interaction of tetraspanin CD9 with α2β1-integrin interferes with membrane anchorage of Rac (Cailleteau *et al.*, 2010), while deletion of CD151 increases RhoA activation (Johnson *et al.*, 2009). CD151 overexpression induces PKC-dependent activation of Rac and Cdc42, but not Rho, promoting cell adhesion (Shigeta *et al.*, 2003). Also, resting levels of Rac activity are lowered in CD81-deficient dendritic cells (Quast *et al.*, 2011). Our current findings thus provide a molecular explanation for the regulation of Rac by TEMs, indicating that CD81 regulates Rac1 dynamics and localization at the cell membrane during membrane protrusion and adhesion formation and establishing a mechanism through which this tetraspanin regulates cell migration.

CD81-Rac complexes were most prominent at the cell leading edge. In this region, Rac promotes actin polymerization and the formation of dendritic actin branches through the activation of the actin-related proteins (Arp2/3) complex via Wiskott–Aldrich syndrome protein (WASP) family Verprolin-homologous protein (WAVE) proteins (Burridge and Wennerberg, 2004). CD81 and other tetraspanins are also commonly used as protein markers of endosomes, lysosomes and exosomes (Simons and Raposo, 2009; Ostrowski *et al.*, 2010). Therefore it is plausible that this interaction also occurs along the export/recycling route.

Most importantly, our data indicate that rather than being necessary for Rac activation or translocation to the membrane, CD81 absence delays its inactivation. Compartmentalization of Rac at the plasma membrane by insertion into TEM might facilitate its binding to a Rho-GDP-dissociation inhibitor (Rho-GDI) protein that targets it for recycling or to a specific Rac-GTPase activating protein (Rac-GAP) or Rac effector. Compartmentalization of Rac at caveolin-rich membrane domains is implicated in its internalization (del Pozo *et al.*, 2005) and degradation (Nethe *et al.*, 2010). Rac interacts directly with caveolin, and depletion of caveolin results in Rac overexpression and hyperactivation (Nethe *et al.*, 2010). Association of Rac with CD81 does not appear to require caveolin, since caveolin was not detected among the proteins pulled down by CD81 C-terminal domain bait peptides. CD81 may thus provide an alternative mode of Rac compartmentalization at the membrane in cells with low or negligible caveolin expression. Importantly, the reduction in CD81 expression may slow Rac deactivation but does not lead to a constitutive activation of the GTPase, since a clear decay is observed at late time points of EGF stimulation. Therefore compartmentalization into TEM emerges as a novel regulatory mechanism of Rac activity turnover.

The increase in basal Rac activity in CD81-silenced cells or in cells pretreated with the permeable peptide correlates with higher protrusion rates and altered adhesion dynamics. Tetraspanins

associate with integrins and partially colocalize with small focal adhesions in the cellular periphery (Berditchevski and Odintsova, 1999). Our results suggest that CD81 may localize Rac to the leading edge anterior to nascent adhesions, thereby controlling Rac availability and favoring the initial steps in adhesion formation. CD81-deficient cells show a facilitated formation of adhesions that is similar to that observed in constitutively active Rac-expressing cells (del Pozo *et al.*, 1999; Rottner *et al.*, 1999; Webb *et al.*, 2004; Choi *et al.*, 2008). However, in contrast with cells expressing a constitutive active form of Rac, the subsequent events of adhesion maturation are not grossly altered in CD81-silenced cells. Thus the combination of faster protrusion and spreading and the facilitation of the initial steps of adhesion formation leads, at later time points, to an increased focal adhesion formation that slows cell motility. Moreover, adhesions in CD81 knocked-down cells are formed beyond the outer rim of the cell, and cytoskeletal polarity is lost, suggesting that CD81-dependent compartmentalization may also be crucial for the spatial regulation of Rac activity and cell polarity. Nevertheless, although cell polarity is perturbed in CD81-silenced cells, the persistence of migration in the absence of any directional cue was very low and no significant differences were observed between the experimental conditions (unpublished data).

Our results map the regulatory effect of CD81 to its C-terminal cytoplasmic region, which strongly suggests that the role of CD81 in controlling cell migration is due to its interaction with Rac rather than its lateral association with other membrane receptors in the context of tetraspanin-enriched microdomains. Moreover, our data with cell-permeable peptides with the sequence of CD81 C-terminal domain suggest that these peptides may be an exciting tool to affect tetraspanin-dependent biological processes in vivo, offering a new, therapeutically valuable application of tetraspanin-targeted reagents for the treatment of malignancies or immune-related diseases.

MATERIALS AND METHODS

Cells

HUVEC were obtained and cultured as described elsewhere (Barreiro *et al.*, 2008). SUM159 breast carcinoma cell line was cultured in DMEM/F-12 (Life Technologies, Invitrogen, Carlsbad, CA), supplemented with 5% fetal bovine serum (FBS), 1% penicillin/streptomycin, nonessential amino acids, 5 μg/ml insulin, and 1 μg/ml hydrocortisone. HEK and U2OS cells were cultured in DMEM (Lonza, Basel, Switzerland) or McCoy's 5A medium (Life Technologies), respectively, both supplemented with 10% FBS and 1% penicillin/streptomycin. HMEC-1 microvascular endothelial cell line was grown in MCDB131 medium (Life Technologies) supplemented with 20% FBS, 1% penicillin/streptomycin, 20 mM HEPES, 2.5 μg/ml fungizone, 10 ng/ml EGF, and 1 μg/ml hydrocortisone.

siRNA

Control siRNA was purchased from Dharmacon (Thermo Scientific, Lafayette, CO). Two different siRNAs for CD81 were purchased from Eurogentec (Seraign, Belgium): CD81b (CACCTTCTATGTAGGCATC) and CD81c (CACGTCGCCTTCAACTGTA). CD81c sequence corresponds to a nontranslated (3'UTR) region of CD81 mRNA, which does not interfere with the expression of exogenous CD81. This sequence was used in rescue experiments.

Antibodies

VJ1/20 (anti-CD9), LIA1/1 (anti-CD151), VJ1/12 (anti-CD59), and HP2/9 (anti-CD44) monoclonal antibodies have been previously described (Yáñez-Mó *et al.*, 1998; Barreiro *et al.*, 2005). Anti-CD81 5A6 was kindly provided by S. Levy (Stanford University, CA), and I.33.22 by R.Vilella (Hospital Clinic, Barcelona). Monoclonal anti-Rac1 (clone 23A8) was purchased from Upstate (now Millipore, Billerica, MA); rabbit policlonal anti-Rac antibody was from Santa Cruz Biotechonology (Santa Cruz, CA), anti-vimentin clone VIM 3B4 from Millipore (Billerica, MA); monoclonal antibody anti-paxillin, reference 03-6100, was from Zymed Laboratories (now Invitrogen, Carlsbad, CA), and clone 177 anti-paxillin was from BD Biosciences (Franklin Lanes, NJ).

Plasmids and reagents

The truncated CD81-ΔCyt-GFP was obtained using the specific primers: CTCGAGATGGGAGTGGAGGGCTGC (5') and AAGCTTACAGCACAGCACCATGCT (3') by PCR onto a CD81 cDNA plasmid. The PCR product was first introduced into the TopoTA vector (Invitrogen) and then subcloned into pAcGFP-N1 or mRFP-N1 (Invitrogen). GFP-wild-type-Rac1, GFP-V12-Rac1 and Orange-paxillin have been previously described (del Pozo *et al.*, 1999).

GST-Rac was provided by X.R. Bustelo (Centro de Investigación del Cancer, Salamanca, Spain); GST-PAK-Crib and C21-GST by J.G. Collard (The Netherlands Cancer Institute, Amsterdam, The Netherlands); and Enhanced Cyan Fluorescent Protein (ECFP)/Ypet-based Raichu-Rac by Y. Wang (University of Illinois, Urbana–Champaign, IL; Ouyang *et al.*, 2008). pTRIP-CD81 (DsRed-CD81) and AqGFP-CD81 (Harris *et al.*, 2008) were provided by J. McKeating (University of Birmingham, UK) and mEmerald-GFP-CD81 (GFP-CD81) and mCherry-CD81 by M.W. Davidson (Florida State University, Tallahassee, FL). All CD81 plasmids had the fluorescent tag in the N-terminal region of the tetraspanin to avoid interference with C-terminal cytoplasmic region conformation or putative function. pEGFP-N1 was from Clontech (Mountain View, CA). EGF was purchased from R&D (Minneapolis, MN) and used at 100 ng/ml at the indicated times. Fibronectin, GTP-γS and GDP were from Sigma-Aldrich (St. Louis, MO).

Tetramethylrhodamine (TAMRA) N-terminal–labeled peptides with the sequences RRRRRRRCCGIRNSSVY (CD81) or RRRRRRRYSVNICRGCSS (Scrambled) were purchased from LifeTein (South Plainfield, NJ).

Pull-down assays

N-terminally biotinylated peptides containing a SGSG linker sequence connected to the cytoplasmic C-terminal domains of the proteins of interest were purchased from Ray Biotech, (Norcross, GA): CD81, biotin-SGSG-CCGIRNSSVY; CD9, biotin-SGSG-CCAIRRNREMV; CD151, biotin-SGSG-YRSLKLEHY; CD82, biotin-SGSG-CRHVHSEDYSKVRKY; EWI-2, biotin-SGSG-CCFMKRLRKR; ICAM-1, biotin-SGSG-RQRKIKKYRLQQAQKGTPMKPTQATPP. Each peptide (30 nmol) was conjugated to 40 μl streptavidin-Sepharose (GE Healthcare, Uppsala, Sweden). Pull-down assays with T-lymphoblasts or HEK extracts were carried out as previously described (Sala-Valdes *et al.*, 2006) and analyzed by Western blotting or mass spectrometry. Briefly, cells were washed once with ice-cold phosphate-buffered saline (PBS) and then lysed in 1% NP-40 in PBS containing protease and phosphatase inhibitors (Complete, PhosSTOP; Roche, Basel, Switzerland). Lysates were precleared for 2 h at 4°C with streptavidin-Sepharose (GE Healthcare) and then incubated for 2 h at 4°C with biotinylated peptides immobilized on streptavidin-Sepharose beads.

For preferential loading of Rac with GDP or GTP, cells were lysed in 5 mM EDTA-containing lysis buffer, and the lysates were incubated with 50 nM of GTP-γS or GDP at 30°C for 5 min before addition of 6 mM MgCl. Alternatively, cells treated, or not, with EGF were lysed in the presence of 2 mM MgCl before incubation with

the Sepharose beads coated with the biotinylated peptides, PAK-GST or C21-GST.

Mass spectrometry

Sepharose beads from the pull-down assays were directly resuspended in Laemmli buffer, applied onto a SDS–PAGE gel, and subjected to the one-step in-gel trypsin digestion method (Bonzon-Kulichenko *et al.*, 2011). The resulting peptides were analyzed by liquid chromatography–tandem mass spectrometry (LC-MS/MS) using a Surveyor LC system coupled to an LTQ linear ion-trap mass spectrometer (Thermo Fisher, San Jose, CA), as previously described (Lopez-Ferrer *et al.*, 2004; Jorge *et al.*, 2009). The LTQ was operated in a data-dependent MS/MS mode using the 15 most intense precursors detected in a survey scan from 400 to 1600 m/z, as previously described (Lopez-Ferrer *et al.*, 2004). Proteins were identified using the SEQUEST algorithm (Bioworks 3.2 package; Thermo Finnigan, Cambridge, MA); the raw MS/MS files were searched against the Human Swissprot database (Uniprot release 14.0, 19929 sequence entries for human) supplemented with the sequence of porcine trypsin. SEQUEST results were validated using the probability ratio method (Martinez-Bartolome *et al.*, 2008), and false discovery rates (FDR) were calculated by the refined method (Navarro and Vázquez, 2009). Peptide and scan counting was performed, assuming as positive events those with a FDR equal to or lower than 5%.

Immunoprecipitation assays

Cells were plated onto 2 µg/ml of fibronectin and serum-starved for at least 6 h when indicated. EGF (100 ng/ml) was applied at the indicated times before lysis in 0.5% Triton-X-100, 60 mM octylglucoside (Sigma-Aldrich) in Tris 10 mM (pH 8), 150 mM NaCl supplemented with protease and phosphatase inhibitors. Antibodies were precoupled to protein G–Sepharose (GE Healthcare), incubated with cell lysates, and washed several times with lysis buffer before being loaded onto an SDS–PAGE gel.

Fluorescence microscopy

For immunofluorescence, cells were fixed with 4% paraformaldehyde (Electron Microscopy Sciences, Hatfield, PA), permeabilized with 0.5% Triton X-100 (5 min), and stained with corresponding primary antibodies followed by species-matching secondary antibodies (Invitrogen). Samples were analyzed in a Leica TCS-SP5 confocal laser-scanning unit equipped with Ar and He/Ne laser beams and attached to a Leica DMIRBE inverted epifluorescence microscope (Leica Microsystems, Heidelberg, Germany); in a TIRF microscope (Leica Microsystems, on a Leica DMI 6000B) using ~100-nm depth penetration; or a wide-field fluorescence Leica DMIRE2 microscope coupled to a monochromator (Polychrome IV; Till Photonics, Munich, Germany) and a CCD camera (CoolSNAP HQ; Photometrics, Tucson, AZ). For time-lapse fluorescence microscopy, cells were maintained at 37°C in 5% CO_2.

For quantification of focal adhesions, subconfluent HUVEC cultures were plated onto 2 µg/ml fibronectin 72 h after transfection, fixed, permeabilized, and stained for paxillin. The area of focal adhesions was selected and measured by Image J using a thresholding method.

Transfection experiments

For DNA or siRNA transfection, cells were electroporated with 2 µM of either negative siRNA or CD81 siRNA duplexes or 20 µg of plasmid DNA, in a Gene Pulser II device (Bio-Rad, Hercules, CA). Conditions used were 200 V, 0.975×10^{-9} Faradays, in 200 µl of standard medium (5 µl of 1.5 M NaCl had been previously supplemented). For rescue experiments, the siRNA duplexes were electroporated together with 20 µg of GFP, GFP-CD81, or CD81-ΔCyt-GFP.

Flow cytometry

CD81 membrane expression was routinely analyzed 48 or 72 h after transfection with siRNA duplexes by immunostaining with anti-CD81 mAb in a FACScan Canto II cytofluorometer (BD Biosciences, Franklin Lanes, NJ), as previously described (Yáñez-Mó *et al.*, 2008). Silencing of CD81 resulted in a reduction of mean fluorescence intensity consistently greater than 50%. In rescue experiments, membrane expression of CD81, stained with an APC-labeled goat anti-mouse, was analyzed after gating GFP-positive cells.

Incorporation of cell-permeable, fluorescently TAMRA-labeled peptides was analyzed in trypsinized unstained cells by flow cytometry.

Fluorescence image cross-correlation analysis

U2OS cells were cotransfected with mCherry-CD81 (wild-type or cytoplasmic deletion mutant) and GFP-Rac1 (wild-type or V12 active mutant). TIRF images were acquired on an Olympus IX71 microscope using a 60×/1.45 numerical aperture (NA) Plan-Apo oil objective and a Ludl controller (Ludl Electronic Products, Hawthorne, NY), and controlled by MetaMorph software (Molecular Devices, Downingtown, PA). GFP and mCherry were excited using a 488-nm line of an argon ion laser (Melles Griot, Albuquerque, NM) and a 561-nm Cobolt Jive ion laser (Market Tech, Scotts Valley, CA), respectively. For simultaneous dual-color imaging, a polychroic mirror (Z488/568 rpc) and dual-emission filter (Z488/568 nm; Chroma Technology, Bellows Falls, VT) were used. Image time series were acquired with a charge-coupled device camera (Retiga Exi; QImaging, Surrey, Canada). Image processing and correlation analysis was performed in MATLAB 7.7.0 (MathWorks, Natick, MA). Images were corrected for background and photobleaching intensity effects. Cell regions ($25 \times 25 - 64 \times 64$ pixels) from both channels were selected for analysis. Single-channel auto- ($a = b = 1$ or 2) and cross-correlation ($a = 1$; $b = 2$) functions were calculated following Wiseman *et al.* (2000):

$$g_{ab}(0,0,\tau) = \frac{\langle \delta i_a(x,y,t)\delta i_b(x,y,t+\tau)\rangle}{\langle \delta i_a\rangle_\tau \langle \delta i_b\rangle_{t+\tau}}$$

where the fluctuation in the fluorescence intensity is defined as

$$\delta i_a(x,y,t) = i_a(x,y,t) - \langle i_a\rangle_\tau$$

$i_a(x,y,t)$ is the fluorescence intensity at a given pixel (x,y) at time t. τ is the temporal lag time. Angular brackets $\langle\cdots\rangle$ denote spatial averaging over the analyzed cell region. The correlation function is normalized by $\langle i_a\rangle_\tau$, the average intensity of the selected region at time t.

Activated Rac measurements

GTP-Rac loading was measured by pulling down GTP-loaded Rac using a GST-coupled PAK-CRIB construct immobilized on Sepharose beads, as described elsewhere (Sander *et al.*, 1999).

Alternatively, endothelial cells were cotransfected with ECFP/Ypet Raichu-Rac and DsRed-CD81 and plated onto 2 µg/ml fibronectin. Cells either untreated or stimulated with 100 ng/ml EGF were imaged using time-lapse confocal microscopy. FRET efficiency is presented as the yellow fluorescent protein (YFP)/cyan fluorescent protein (CFP) ratio after CFP stimulation, as previously described (Ouyang *et al.*, 2008).

Protrusion rate and adhesion turnover measurements

SUM159 cells were either transfected with GFP or CD81-GFP, cotransfected with control or CD81 siRNA and GFP, or transfected with GFP and incubated 2 h with 1 μM permeable CD81 or scrambled peptides. Cells were then trypsinized, washed, and plated onto 35-mm dishes (MatTek) coated with 10 μg/ml of fibronectin. Images were acquired for 10 min with 1 frame every 5 s using a Leica AM TIRF MC mounted on a Leica DMI6000B microscope fitted with a 100×/1.46 NA oil-immersion objective with 1× magnification and ~90-nm penetration depth. The protrusion rate was measured with Image J's Multiple Kymograph plug-in, as described elsewhere (Choi *et al.*, 2008).

For the study of focal adhesion turnover, cells cotransfected with Orange-paxillin, together with control or CD81siRNA and GFP, GFP-CD81, or CD81-ΔCyt-GFP, were allowed to spread, and adhesion assembly and disassembly rates were analyzed with Image J, as previously described (Webb *et al.*, 2004; Choi *et al.*, 2008).

Spreading assays on micropatterned substrates

Micropatterned slides were purchased from CYTOO (Grenoble, France). Cells were trypsinized and replated onto micropatterned slides (CYTOO Starter), according to the manufacturer's instructions. Cells were allowed to attach and spread for 3 h and were then fixed with paraformaldehyde, permeabilized, and stained for paxillin or F-actin. Images were acquired using wide-field fluorescence microscopy and analyzed with the Image J Reference-cell macro. Briefly, images were cropped following the micropatterned image and micropatterns containing multiple cells were discarded by nuclei counting. Average projections of the label image of several individual cells (paxillin or F-actin) are presented in a pseudocolor intensity-scale image.

Migration experiments

SUM159 cells were plated on fibronectin (2 μg/ml) 2 d after transfection and serum-starved for 12 h. Alternatively, SUM159 were plated on fibronectin (2 μg/ml) and incubated for 1 h with 1 μM permeable CD81 or scrambled peptides. Images were acquired at 10-min intervals for 24 h in a Nikon Eclipse Ti-E video microscope (Tokyo, Japan). Tracking of transfected cells was performed with Image J and MetaMorph software.

Statistical analysis

Statistical significance was calculated using Student's *t* test or one-way analysis of variance (ANOVA), and significant differences were labeled as: *, $p < 0.05$; **, $p < 0.01$; and ***, $p < 0.001$.

ACKNOWLEDGMENTS

We thank M. Vicente-Manzanares and M. Gómez for critical reading of the manuscript. Microscopy was partially conducted at the CNIC-Microscopy & Dynamic Imaging Unit. This work was supported by grants PI080794 and PI11/01645 from the Instituto de Salud Carlos III to M.Y.-M.; SAF2011-25834 and ERC AdG-2011 to F.S.M; BIO2009-07990 from the Ministerio de Educación y Ciencia, CAM BIO/0194/2006 from Comunidad de Madrid, and RECAVA RD06/0014 from the Fondo de Investigaciones Sanitarias (Ministerio de Sanidad y Consumo, Instituto Salud Carlos III) to J.V. and F.S.-M. A.R.H. was supported by National Institutes of Health grant GM23244 and the Cell Migration Consortium (U54 GM064346).

REFERENCES

Barreiro O, Yáñez-Mó M, Sala-Valdes M, Gutierrez-Lopez MD, Ovalle S, Higginbottom A, Monk PN, Cabanas C, Sánchez-Madrid F (2005). Endothelial tetraspanin microdomains regulate leukocyte firm adhesion during extravasation. Blood 105, 2852–2861.

Barreiro O, Zamai M, Yáñez-Mó M, Tejera E, Lopez-Romero P, Monk PN, Gratton E, Caiolfa VR, Sánchez-Madrid F (2008). Endothelial adhesion receptors are recruited to adherent leukocytes by inclusion in preformed tetraspanin nanoplatforms. J Cell Biol 183, 527–542.

Berditchevski F (2001). Complexes of tetraspanins with integrins: more than meets the eye. J Cell Sci 114, 4143–4151.

Berditchevski F, Odintsova E (1999). Characterization of integrin-tetraspanin adhesion complexes: role of tetraspanins in integrin signaling. J Cell Biol 146, 477–492.

Berditchevski F, Tolias KF, Wong K, Carpenter CL, Hemler ME (1997). A novel link between integrins, transmembrane-4 superfamily proteins (CD63 and CD81), and phosphatidylinositol 4-kinase. J Biol Chem 272, 2595–2598.

Bonzon-Kulichenko E *et al.* (2011). A robust method for quantitative high-throughput analysis of proteomes by 18O labeling. Mol Cell Proteomics 10, M110.003335.

Brown CM, Hebert B, Kolin DL, Zareno J, Whitmore L, Horwitz AR, Wiseman PW (2006). Probing the integrin-actin linkage using high-resolution protein velocity mapping. J Cell Sci 119, 5204–5214.

Burridge K, Wennerberg K (2004). Rho and Rac take center stage. Cell 116, 167–179.

Cailleteau L *et al.* (2010). α2β1 integrin controls association of Rac with the membrane and triggers quiescence of endothelial cells. J Cell Sci 123, 2491–2501.

Carloni V, Mazzocca A, Ravichandran KS (2004). Tetraspanin CD81 is linked to ERK/MAP kinase signaling by Shc in liver tumor cells. Oncogene 23, 1566–1574.

Charrin S, le Naour F, Silvie O, Milhiet PE, Boucheix C, Rubinstein E (2009). Lateral organization of membrane proteins: tetraspanins spin their web. Biochem J 420, 133–154.

Choi CK, Vicente-Manzanares M, Zareno J, Whitmore LA, Mogilner A, Horwitz AR (2008). Actin and α-actinin orchestrate the assembly and maturation of nascent adhesions in a myosin II motor-independent manner. Nat Cell Biol 10, 1039–1050.

Choi CK, Zareno J, Digman MA, Gratton E, Horwitz AR (2011). Cross-correlated fluctuation analysis reveals phosphorylation-regulated paxillin-FAK complexes in nascent adhesions. Biophys J 100, 583–592.

Clark KL, Oelke A, Johnson ME, Eilert KD, Simpson PC, Todd SC (2004). CD81 associates with 14-3-3 in a redox-regulated palmitoylation-dependent manner. J Biol Chem 279, 19401–19406.

del Pozo MA, Balasubramanian N, Alderson NB, Kiosses WB, Grande-Garcia A, Anderson RG, Schwartz MA (2005). Phospho-caveolin-1 mediates integrin-regulated membrane domain internalization. Nat Cell Biol 7, 901–908.

del Pozo MA, Vicente-Manzanares M, Tejedor R, Serrador JM, Sánchez-Madrid F (1999). Rho GTPases control migration and polarization of adhesion molecules and cytoskeletal ERM components in T lymphocytes. Eur J Immunol 29, 3609–3620.

Digman MA, Wiseman PW, Horwitz AR, Gratton E (2009). Detecting protein complexes in living cells from laser scanning confocal image sequences by the cross correlation raster image spectroscopy method. Biophys J 96, 707–716.

Dijkstra S, Kooij G, Verbeek R, van der Pol SM, Amor S, Geisert EE, Jr., Dijkstra CD, van Noort JM, Vries HE (2008). Targeting the tetraspanin CD81 blocks monocyte transmigration and ameliorates EAE. Neurobiol Dis 31, 413–421.

Domanico SZ, Pelletier AJ, Havran WL, Quaranta V (1997). Integrin α6Aβ1 induces CD81-dependent cell motility without engaging the extracellular matrix migration substrate. Mol Biol Cell 8, 2253–2265.

Garcia-Lopez MA, Barreiro O, Garcia-Diez A, Sánchez-Madrid F, Penas PF (2005). Role of tetraspanins CD9 and CD151 in primary melanocyte motility. J Invest Dermatol 125, 1001–1009.

Guo F, Cancelas JA, Hildeman D, Williams DA, Zheng Y (2008). Rac GTPase isoforms Rac1 and Rac2 play a redundant and crucial role in T-cell development. Blood 112, 1767–1775.

Harris HJ *et al.* (2008). CD81 and claudin 1 coreceptor association: role in hepatitis C virus entry. J Virol 82, 5007–5020.

Hemler ME (2003). Tetraspanin proteins mediate cellular penetration, invasion, and fusion events and define a novel type of membrane microdomain. Annu Rev Cell Dev Biol 19, 397–422.

Hong IK, Jin YJ, Byun HJ, Jeoung DI, Kim YM, Lee H (2006). Homophilic interactions of tetraspanin CD151 up-regulate motility and matrix metalloproteinase-9 expression of human melanoma cells through adhesion-dependent c-Jun activation signaling pathways. J Biol Chem 281, 24279–24292.

Johnson JL, Winterwood N, DeMali KA, Stipp CS (2009). Tetraspanin CD151 regulates RhoA activation and the dynamic stability of carcinoma cell-cell contacts. J Cell Sci 122, 2263–2273.
Jorge I, Navarro P, Martinez-Acedo P, Nunez E, Serrano H, Alfranca A, Redondo JM, Vázquez J (2009). Statistical model to analyze quantitative proteomics data obtained by 18O/16O labeling and linear ion trap mass spectrometry: application to the study of vascular endothelial growth factor-induced angiogenesis in endothelial cells. Mol Cell Proteomics 8, 1130–1149.
Kramer B *et al*. (2009). Regulation of NK cell trafficking by CD81. Eur J Immunol 39, 3447–3458.
Lagaudriere-Gesbert C, Le Naour F, Lebel-Binay S, Billard M, Lemichez E, Boquet P, Boucheix C, Conjeaud H, Rubinstein E (1997). Functional analysis of four tetraspans, CD9, CD53, CD81, and CD82, suggests a common role in costimulation, cell adhesion, and migration: only CD9 upregulates HB-EGF activity. Cell Immunol 182, 105–112.
Latysheva N, Muratov G, Rajesh S, Padgett M, Hotchin NA, Overduin M, Berditchevski F (2006). Syntenin-1 is a new component of tetraspanin-enriched microdomains: mechanisms and consequences of the interaction of syntenin-1 with CD63. Mol Cell Biol 26, 7707–7718.
Lopez-Ferrer D, Martinez-Bartolome S, Villar M, Campillos M, Martin-Maroto F, Vázquez J (2004). Statistical model for large-scale peptide identification in databases from tandem mass spectra using SEQUEST. Anal Chem 76, 6853–6860.
Martinez-Bartolome S, Navarro P, Martin-Maroto F, Lopez-Ferrer D, Ramos-Fernandez A, Villar M, Garcia-Ruiz JP, Vázquez J (2008). Properties of average score distributions of SEQUEST: the probability ratio method. Mol Cell Proteomics 7, 1135–1145.
Mazzocca A, Liotta F, Carloni V (2008). Tetraspanin CD81-regulated cell motility plays a critical role in intrahepatic metastasis of hepatocellular carcinoma. Gastroenterology 135, 244–256.
Mela A, Goldman JE (2009). The tetraspanin KAI1/CD82 is expressed by late-lineage oligodendrocyte precursors and may function to restrict precursor migration and promote oligodendrocyte differentiation and myelination. J Neurosci 29, 11172–11181.
Moissoglu K, Slepchenko BM, Meller N, Horwitz AF, Schwartz MA (2006). In vivo dynamics of Rac-membrane interactions. Mol Biol Cell 17, 2770–2779.
Nattermann J, Zimmermann H, Iwan A, von Lilienfeld-Toal M, Leifeld L, Nischalke HD, Langhans B, Sauerbruch T, Spengler U (2006). Hepatitis C virus E2 and CD81 interaction may be associated with altered trafficking of dendritic cells in chronic hepatitis. Hepatology C 44, 945–954.
Navarro P, Vázquez J (2009). A refined method to calculate false discovery rates for peptide identification using decoy databases. J Proteome Res 8, 1792–1796.
Nethe M, Anthony EC, Fernandez-Borja M, Dee R, Geerts D, Hensbergen PJ, Deelder AM, Schmidt G, Hordijk PL (2010). Focal-adhesion targeting links caveolin-1 to a Rac1-degradation pathway. J Cell Sci 123, 1948–1958.
Ostrowski M *et al*. (2010). Rab27a and Rab27b control different steps of the exosome secretion pathway. Nat Cell Biol 12, 19–3011–13.
Ouyang M, Sun J, Chien S, Wang Y (2008). Determination of hierarchical relationship of Src and Rac at subcellular locations with FRET biosensors. Proc Nat Acad Sci USA 105, 14353–14358.
Penas PF, Garcia-Diez A, Sánchez-Madrid F, Yáñez-Mó M (2000). Tetraspanins are localized at motility-related structures and involved in normal human keratinocyte wound healing migration. J Invest Dermatol 114, 1126–1135.
Quast T, Eppler F, Semmling V, Schild C, Homsi Y, Levy S, Lang T, Kurts C, Kolanus W (2011). CD81 is essential for the formation of membrane protrusions and regulates Rac1-activation in adhesion-dependent immune cell migration. Blood 118, 1818–1827.
Rottner K, Hall A, Small JV (1999). Interplay between Rac and Rho in the control of substrate contact dynamics. Curr Biol 9, 640–648.
Sala-Valdes M, Ailane N, Greco C, Rubinstein E, Boucheix C (2012). Targeting tetraspanins in cancer. Expert Opin Ther Targets 16, 985–997.
Sala-Valdes M, Ursa A, Charrin S, Rubinstein E, Hemler ME, Sánchez-Madrid F, Yáñez-Mó M (2006). EWI-2 and EWI-F link the tetraspanin web to the actin cytoskeleton through their direct association with ezrin-radixin-moesin proteins. J Biol Chem 281, 19665–19675.
Sander EE, ten Klooster JP, van Delft S, van der Kammen RA, Collard JG (1999). Rac downregulates Rho activity: reciprocal balance between both GTPases determines cellular morphology and migratory behavior. J Cell Biol 147, 1009–1022.
Shigeta M, Sanzen N, Ozawa M, Gu J, Hasegawa H, Sekiguchi K (2003). CD151 regulates epithelial cell-cell adhesion through PKC- and Cdc42-dependent actin cytoskeletal reorganization. J Cell Biol 163, 165–176.
Simons M, Raposo G (2009). Exosomes—vesicular carriers for intercellular communication. Curr Opin Cell Biol 21, 575–581.
Takeda Y *et al*. (2008). Double deficiency of tetraspanins CD9 and CD81 alters cell motility and protease production of macrophages and causes chronic obstructive pulmonary disease-like phenotype in mice. J Biol Chem 283, 26089–26097.
Takeda Y, Kazarov AR, Butterfield CE, Hopkins BD, Benjamin LE, Kaipainen A, Hemler ME (2007). Deletion of tetraspanin Cd151 results in decreased pathologic angiogenesis in vivo and in vitro. Blood 109, 1524–1532.
Tan JL, Liu W, Nelson CM, Raghavan S, Chen CS (2004). Simple approach to micropattern cells on common culture substrates by tuning substrate wettability. Tissue Eng 10, 865–872.
Tarrant JM, Robb L, van Spriel AB, Wright MD (2003). Tetraspanins: molecular organisers of the leukocyte surface. Trends Immunol 24, 610–617.
Tham TN, Gouin E, Rubinstein E, Boucheix C, Cossart P, Pizarro-Cerda J (2010). Tetraspanin CD81 is required for *Listeria monocytogenes* invasion. Infect Immun 78, 204–209.
Thery M, Racine V, Piel M, Pepin A, Dimitrov A, Chen Y, Sibarita JB, Bornens M (2006). Anisotropy of cell adhesive microenvironment governs cell internal organization and orientation of polarity. Proc Natl Acad Sci USA 103, 19771–19776.
Webb DJ, Donais K, Whitmore LA, Thomas SM, Turner CE, Parsons JT, Horwitz AF (2004). FAK-Src signalling through paxillin, ERK and MLCK regulates adhesion disassembly. Nat Cell Biol 6, 154–161.
Wiseman PW, Brown CM, Webb DJ, Hebert B, Johnson NL, Squier JA, Ellisman MH, Horwitz AF (2004). Spatial mapping of integrin interactions and dynamics during cell migration by image correlation microscopy. J Cell Sci 117, 5521–5534.
Wiseman PW, Squier JA, Ellisman MH, Wilson KR (2000). Two-photon image correlation spectroscopy and image cross-correlation spectroscopy. J Microsc 200, 14–25.
Yamada M, Sumida Y, Fujibayashi A, Fukaguchi K, Sanzen N, Nishiuchi R, Sekiguchi K (2008). The tetraspanin CD151 regulates cell morphology and intracellular signaling on laminin-511. FEBS J 275, 3335–3351.
Yáñez-Mó M, Alfranca A, Cabanas C, Marazuela M, Tejedor R, Ursa MA, Ashman LK, de Landazuri MO, Sánchez-Madrid F (1998). Regulation of endothelial cell motility by complexes of tetraspan molecules CD81/TAPA-1 and CD151/PETA-3 with $\alpha 3\beta 1$ integrin localized at endothelial lateral junctions. J Cell Biol 141, 791–804.
Yáñez-Mó M *et al*. (2008). MT1-MMP collagenolytic activity is regulated through association with tetraspanin CD151 in primary endothelial cells. Blood 112, 3217–3226.
Yáñez-Mó M, Barreiro O, Gordon-Alonso M, Sala-Valdes M, Sánchez-Madrid F (2009). Tetraspanin-enriched microdomains: a functional unit in cell plasma membranes. Trends Cell Biol 19, 434–446.
Yáñez-Mó M, Gutierrez-Lopez MD, Cabanas C (2011). Functional interplay between tetraspanins and proteases. Cell Mol Life Sci 68, 3323–3335.
Yáñez-Mó M, Mittelbrunn M, Sánchez-Madrid F (2001a). Tetraspanins and intercellular interactions. Microcirculation 8, 153–168.
Yáñez-Mó M, Tejedor R, Rousselle P, Sanchez–Madrid F (2001b). Tetraspanins in intercellular adhesion of polarized epithelial cells: spatial and functional relationship to integrins and cadherins. J Cell Sci 114, 577–587.
Yauch RL, Hemler ME (2000). Specific interactions among transmembrane 4 superfamily (TM4SF) proteins and phosphoinositide 4-kinase. Biochem J 351, 629–637.
Zhang XA, Bontrager AL, Hemler ME (2001a). Transmembrane-4 superfamily proteins associate with activated protein kinase C (PKC) and link PKC to specific β_1 integrins. J Biol Chem 276, 25005–25013.
Zhang XA, Bontrager AL, Stipp CS, Kraeft SK, Bazzoni G, Chen LB, Hemler ME (2001b). Phosphorylation of a conserved integrin $\alpha 3$ QPSXXE motif regulates signaling, motility, and cytoskeletal engagement. Mol Biol Cell 12, 351–365.